Clim Dyn (2011) 36:1505–1521
DOI 10.1007/s00382-009-0723-4

Aridity changes in the Temperate-Mediterranean transition of the Andes since AD 1346 reconstructed from tree-rings

Duncan A. Christie · José A. Boninsegna · Malcolm K. Cleaveland · Antonio Lara · Carlos Le Quesne · Mariano S. Morales · Manfred Mudelsee · David W. Stahle · Ricardo Villalba

Received: 3 September 2009 / Accepted: 5 December 2009 / Published online: 23 December 2009

Abstract The Andes Cordillera acts as regional "Water Towers" for several countries and encompasses a wide range of ecosystems and climates. Several hydroclimatic changes have been described for portions of the Andes during recent years, including glacier retreat, negative precipitation trends, an elevation rise in the 0° isotherm, and changes in regional streamflow regimes. The Temperate-Mediterranean transition (TMT) zone of the Andes (35.5°–39.5°S) is particularly at risk to climate change because it is a biodiversity hotspot with heavy human population pressure on water resources. In this paper we utilize a new tree-ring network of *Austrocedrus chilensis* to reconstruct past variations in regional moisture in the TMT of the Andes by means of the Palmer Drought Severity Index (PDSI). The reconstruction covers the past 657 years and captures interannual to decadal scales of variability in late spring–early summer PDSI. These changes are related to the north–south oscillations in moisture conditions between the Mediterranean and Temperate climates of the Andes as a consequence of the latitudinal position of the storm tracks forced by large-scale circulation modes. Kernel estimation of occurrence rates reveals an unprecedented increment of severe and extreme drought events during the last century in the context of the previous six centuries. Moisture conditions in our study region are linked to tropical and high-latitude ocean-atmospheric forcing, with PDSI positively related to Niño-3.4 SST during spring and strongly negatively correlated with the Antarctic Oscillation (AAO) during summer. Geopotential anomaly maps at 500-hPa show that extreme dry years are tightly associated with negative height anomalies in the Ross–Amundsen Seas, in concordance with the strong negative relationship between PDSI and AAO. The twentieth century increase in extreme drought events in the TMT may not be related to ENSO but to the positive AAO trend during late-spring and summer resulting from a gradual poleward shift of the mid-latitude storm tracks. This first PDSI reconstruction for South America demonstrates the highly significant hindcast skill of *A. chilensis* as an aridity proxy.

Keywords South-central Andes · Climatic transition · Palmer Drought Severity Index · Tree-rings · *Austrocedrus chilensis* · Climate change · AAO

D. A. Christie (✉) · A. Lara · C. Le Quesne
Laboratorio de Dendrocronología, Facultad de Ciencias Forestales y Recursos Naturales, Universidad Austral de Chile, Casilla 567, Valdivia, Chile
e-mail: duncanchristieb@gmail.com

J. A. Boninsegna · M. S. Morales · R. Villalba
Departamento de Dendrocronología e Historia Ambiental, Instituto Argentino de Nivología, Glaciología y Ciencias Ambientales, IANIGLA, C.C. 330, 5500 Mendoza, Argentina

M. K. Cleaveland · D. W. Stahle
Tree-Ring Laboratory, Department of Geosciences, University of Arkansas Fayetteville, Ozark Hall 113, Fayetteville, AR 72701, USA

A. Lara
Forest Ecosystem Services under Climatic Fluctuations (Forecos), Universidad Austral de Chile, Valdivia, Chile

M. Mudelsee
Climate Risk Analysis, Schneiderberg 26, 30167 Hanover, Germany

M. Mudelsee
Alfred Wegener Institute for Polar and Marine Research, Bussestrasse 24, 27570 Bremerhaven, Germany

1 Introduction

The Andes Cordillera is one of the largest mountain ranges on earth extending from the northern tropics of South America ~8°N all the way to the southern tip of Patagonia at ~55°S in a territory that spans a myriad of climates and ecosystems, including absolute desert, tropical forests, and ice fields (Aceituno et al. 1983; Young and León 2006; Armesto et al. 1996; Veblen et al. 2007; Garreaud et al. 2009). The latitudinal variation in climatic regions along the Andes is dramatic, and the sharp gradient between the warm/water-limited Mediterranean and the cool/wet temperate climate types is located within a narrow latitudinal band on the western margin of South America from 35.5° to 39.5°S, forming the Temperate-Mediterranean transition (TMT) zone of the Andes (Villagrán and Hinojosa 1997).

Drought in the TMT of the Andes has significant socio-economic and ecological impacts (Masiokas et al. 2006). The Cordillera acts as a regional water tower where >70% of the national hydropower of Chile is produced (INE 2004). This ecotonal region is also a biodiversity hotspot with high levels of species richness and endemism (Villagrán and Hinojosa 1997; Myers et al. 2000; Samaniego and Marquet 2009), and the second most human populated area in Chile. The available hydrological resources in the TMT of the Andes are currently being stressed due to the decreasing trend of up to 30% in the observed precipitation (Carrasco et al. 2005), the increase in elevation of the 0°C isotherm (Carrasco et al. 2008), sustained glacial retreat (Masiokas et al. 2009b), and changes in the snowmelt-dominated streamflow regime towards an earlier annual center of mass (Cortés et al. 2008). These environmental changes have occurred in conjunction with intense land-use changes (Echeverría et al. 2006) and a growing demand for water and natural resources as a result of population increase and economic growth (Giglo 2006). Predictive atmospheric circulation models indicate that precipitation will significantly decrease while temperature in the lower troposphere and the elevation of the 0°C isotherm will substantially increase over the next 100 years in this ecoregion (Carrasco et al. 2005; Bradley et al. 2006; Christensen et al. 2007; Fuenzalida et al. 2007).

Investigations of the temporal and spatial variations of drought in the TMT of the Andes are a high research priority for the detection and attribution of climate change (sensu Hegerl et al. 2007). However, the instrumental climatic records for this Andean sector generally begin after 1920. Longer high-resolution palaeoclimate records are needed to understand how the interannual modes of climate variability have evolved with long-term changes in the background climate (Jansen et al. 2007). Tree-rings from *Austrocedrus chilensis* should be an excellent proxy for reconstructing past drought variability in the TMT of the Andes given it exactly dated annual resolution and the demonstrated sensitivity to moisture variations in the Mediterranean (32°–35°S) and Temperate Rain Andes (39°–43°S) (LaMarche 1978; Boninsegna 1988; Villalba et al. 1998; Le Quesne et al. 2006; 2008; Lara et al. 2008; Boninsegna et al. 2009). Accurate, long-term drought reconstructions for the TMT would help quantify the nature of ongoing climate changes and could provide information to test and verify climate circulation models (Randall et al. 2007; Lohmann 2008).

The main goal of the present study was to develop an exactly dated annual resolution drought record for the TMT of the Andes, based on a new multicentury Andean network of *A. chilensis* tree-ring chronologies and using the most common drought metric, the Palmer Drought Severity Index (PDSI; Palmer 1965). We utilized this long proxy drought record, the first PDSI tree-ring reconstruction for the Southern Hemisphere to: (1) describe a key component of late-spring early summer climate history of the TMT of the Andes for the past seven centuries, (2) determine the spatial patterns of drought in this climatic transition zone, (3) determine the occurrence rate of drought extremes, (4) asses the relationship of drought with tropical and high-latitude ocean-atmospheric forcing, and (5) compare the drought signal periodicities of this reconstruction with palaeo-hydroclimatic records from the adjacent Mediterranean and Temperate Andes.

2 The Temperate-Mediterranean transition of the Andes

The TMT of the Andes is a narrow latitudinal band (35.5°–39.5°S) located on the western margin of South America encompassing the Andes and the strip of Chilean territory to the west (Fig. 1). This climatic region is defined by the transition between the semi-arid Mediterranean (32°–35.5°S) to the temperate rain climate zones (39.5°–55.5°S), the latter being one of the wettest extra-tropical regions in the world (Miller 1976). Precipitation in the TMT is concentrated during fall and winter (~70% of the annual total), and there is a sharp north–south increase in annual precipitation from ~1,000 mm in the north to ~3,000 mm in the south. Mean annual temperature declines less sharply, from 14.8°C in the north to 11.9°C in the south (Miller 1976). Rainy events are mainly associated with cold and warm fronts which affect the narrow territory between the Pacific coast and the Andes Cordillera (Fig. 1; Garreaud 2007). The sharp precipitation gradient is due to the steady increase in both the frequency and intensity of the westerly winds with increasing latitude from the Mediterranean to the Temperate Rain region (Garreaud et al. 2009). This is reflected by both heavier

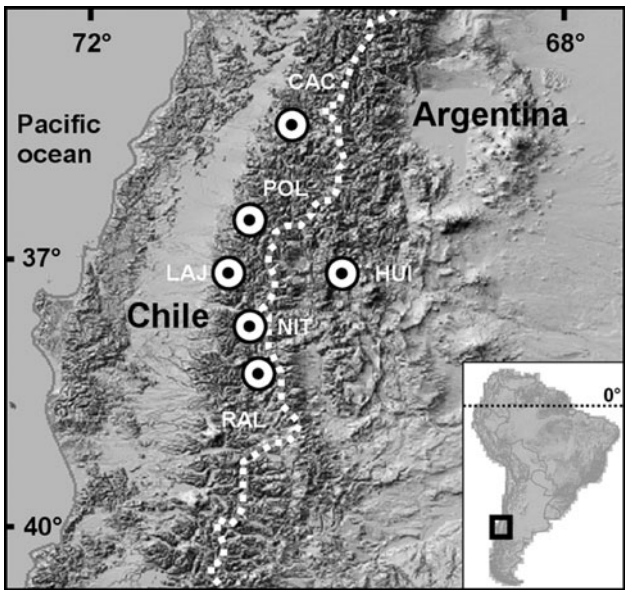

Fig. 1 Location map of the study sites in the Temperate-Mediterranean transition (TMT) of the Andes (35.5°–39.5°S). *White dots* and *codes* indicate six tree-ring sites, and the *white dotted line* the Chilean-Argentinean border which follows the continental divide

rainfall and wetter summer months towards the south (Miller 1976). Moreover, the interannual variability in precipitation is inversely correlated with latitude, reflecting the variable nature of precipitation over the Mediterranean region (Garreaud et al. 2009). In the TMT region, the Andes acts as an impressive topographic barrier to the persistent westerly humid air masses that dominate circulation in this area. This mountain range prevents the intrusion of Atlantic air-masses creating a gradient from a wetter zone on the windward western slope to a drier region on the eastern (leeward) side of the Cordillera, resulting in a decline in annual precipitation from $\sim$1, 200 to 3,000 mm on the Chilean side to less than 250 mm 40 km east of the Andes (Miller 1976).

Interactions between tropical and high-latitude modes of ocean-atmospheric circulation determine the intra- as well as inter-annual precipitation variability in the TMT. Intra-seasonal rainfall variability is modulated directly by changes in the position and/or intensity of storm tracks reflecting the large-scale zonal wind variability, forced either by tropical or high-latitude circulation modes (Garreaud 2007). At the interannual time-scale, the combined effect of El Niño-Southern Oscillation (ENSO) warm events and high-pressure blockings around Antarctica enhances the tropical-extratropical temperature gradient which in turn contributes to the northward migration of the storm tracks and positive precipitation anomalies during late-spring in the TMT (Montecinos and Aceituno 2003). Conversely, extremely dry years coincide with a reversed pressure gradient between mid-latitude and Antarctic regions during cold ENSO events (Garreaud et al. 2009).

The sharp latitudinal precipitation gradient in the TMT creates a natural ecological boundary for several plant and animal species which converge from the Temperate and Mediterranean domains. Up to 70% of the vascular flora in Chile is found in this transitional ecoregion (Villagrán and Hinojosa 1997). The TMT of the Andes has been impacted by human activity since pre-Colombian times, when the region supported one of the largest native cultures of the Chilean zone (Dillehay 2007). The human-impact dramatically increased after the arrival of the Spanish conquerors during the mid 1500s, and especially from the eighteenth century onwards when intensive forest logging and agricultural activity changed the land-use patterns (Camus 2006). Since the 1970s, the diverse native forests ecosystems have been widely replaced by exotic *Eucalyptus* spp and *Pinus radiata* plantations subsidized by the Chilean government, resulting in vast areas of the TMT suffering some of the highest deforestation rates in the world (Lara and Veblen 1993; Bustamante and Castor 1998; Echeverría et al. 2006). Today, the TMT of the Andes has been cited as one of the global biodiversity hotspots most threatened by human activity (Myers et al. 2000; Rodriguez-Cabal et al. 2008; Underwood et al. 2008).

3 The PDSI reconstruction method

3.1 The tree-ring network

In the south-central Andes and following the western margin of the Arid Diagonal, a narrow band of scarce precipitation crossing South America from the east-coast of Patagonia up to northern Peru (Abraham et al. 2000), grows the conifer *A. chilensis* (32.6°–43.8°S; Fig. 2). This drought-adapted species has clear annual growth rings and can live for more than 1,200 years. Tree-ring chronologies of *A. chilensis* have been widely used to reconstruct past hydroclimate variability since the 1970s, including precipitation (LaMarche 1978; Boninsegna 1988; Villalba et al. 1998; Le Quesne et al. 2006; 2008), and streamflow (Holmes et al. 1979; Cobos and Boninsegna 1983; Lara et al. 2008). In this study, we took advantage of the extreme moisture sensitivity of this species to reconstruct past drought variability as measured by the PDSI in the TMT of the Andes.

We developed a highly replicated tree-ring network of *A. chilensis* sampling six populations on both flanks of the Andes, in Chile and Argentina (Table 1). The sampling sites were carefully selected to climatically represent the narrow latitudinal band of the TMT and at the same time

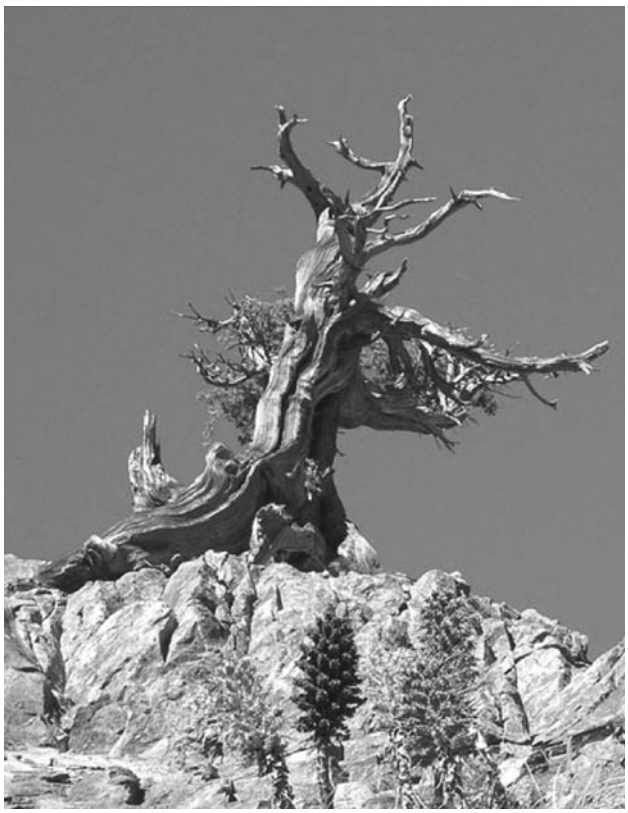

Fig. 2 Ancient *Austrocedrus chilensis* (Ciprés de Cordillera) individual growing on a rocky site

capture the north–south and east–west moisture gradients (Fig. 1). Interestingly, on the much drier eastern slope of the Andes, the Huinganco site (37°S) has a relict population representing the northernmost limit of *A. chilensis* on the leeward flank of the Cordillera (Boninsegna and Holmes 1978). In contrast, the range of this species extends up to ~33°S on the windward Andean slope.

Increment cores from living trees and cross-sections from dead trees and sub-fossil wood were collected from open stands located on steep, rocky, and xeric environments, totaling about 650 tree-ring series that include ~162,300 annual ring measurements. Samples were prepared following standard dendrochronological techniques as outlined in Stokes and Smiley (1968). Tree-rings were visually cross-dated to the year of ring formation (Fritts 1976) and measured under a binocular stereoscope with 0.001 mm precision. We followed the Schulman (1956) convention for the Southern Hemisphere which assigns dates of annual rings to the year in which the radial growth started. The cross-dating quality and measurement accuracy of the tree-ring samples were checked with the computer program COFECHA (Holmes 1983). Individual ring-width measurements were detrended to remove variability in the time series not related to climate such as tree aging or forest disturbances. The measured ring width of year t was divided by the year t value of a fitted negative exponential curve or a linear regression (Fritts 1976). Ring-width chronologies were calculated averaging the detrended tree-ring series of each *A. chilensis* site with a biweight robust mean estimation by the ARSTAN40c program (Cook and Krusic 2006). The variance of the chronologies was stabilized using the method described by Osborn et al. (1997). The quality of the tree-ring chronologies was assessed by using the statistic expressed population signal (EPS). To calculate EPS, we used a 30-years window with an overlap of 15 years between adjacent windows. The EPS measures the strength of the trees common signal in a chronology over time and quantifies the degree to which it portrays the hypothetically perfect chronology (Wigley et al. 1984). While there is no level of significance for EPS per se, we utilized the commonly applied 0.85 threshold to denote a good level of common signal fidelity between trees and used only this portion of the chronologies as predictors in the reconstruction. The common period of all the chronologies with an EPS above 0.85 is 1663–2000 with a mean of the correlations of each chronology with all the others ranging from 0.24 to 0.67 (Table 1). As an exploratory analysis of our tree-ring network we performed an Empirical Orthogonal Function (EOF) between the tree-ring chronologies over the 1663–2000 common period to asses the main modes of tree-growth variability with its associated spatial patterns. The results allowed us to confirm that the selection of sample sites exactly represented what we expected with a first leading EOF explaining a large portion of the common variance (69%) where all chronologies have relatively similar loadings demonstrating a strong regional environmental signal contained in all sites (Fig. 3). In the same manner the second and third EOF highlight the east–west and north–south moisture gradient of the TMT, respectively, however as unrotated EOF's are not domain-shape independent, the interpretation of these two modes should be taken with caution. These results clearly demonstrated that the location and signal recorded in our tree-ring network represent the homogeneous climate of the TMT as well as the secondary moisture gradients contained in it.

3.2 Calibration and verification of PDSI

As the target drought metric, we used the monthly 2.5° × 2.5° gridded PDSI data from Dai et al. (2004). The PDSI is an extensively used measure of regional moisture availability and its computation is based on a water supply and demand model calculated using instrumental records of precipitation and temperature and the soil characteristics of the study region, resulting in an index classified according to 11 categories (Table 2; Palmer 1965). The calculation of the index involves the quantities of potential

Table 1 Characteristics of *Austrocedrus chilensis* tree-ring chronologies from the Temperate-Mediterranean transition of the Andes

Site name and code	Lat S, long W	Elev (m)	Country	No. series	Period[a]	Corr[b]	Correlations[c]	
							t	$t+2$
Melado, CAC	35°52′, 71°00′	1,435	Chile	108	1429–2004	0.59	0.34	−0.25
Polcura, POL	37°04′, 71°24′	1,205	Chile	131	1346–2004	0.69	0.55	−0.28
Huinganco, HUI	37°45′, 70°36′	1,450	Argentina	101	1070–2000	0.48	0.24	–
Laja, LAJ	37°19′, 71°32′	740	Chile	103	1489–2004	0.61	0.61	−0.30
Nitrao, NIT	37°41′, 71°17′	1,220	Chile	109	1433–2004	0.68	0.58	−0.31
Ralko-Lepoy, RAL	38°03′, 71°18′	1,080	Chile	90	1663–2004	0.67	0.67	–

[a] >0.85 EPS value

[b] Mean of the correlations of each tree-ring chronology with all the others for their 1663-2000 common period ($P < 0.001$; $n = 338$)

[c] Significant correlations between each tree-ring chronology and late-spring early summer (December) PDSI over the 1940–2000 period for lags t and $t + 2$ ($P < 0.05$), no chronology was significantly correlated at $t + 1$

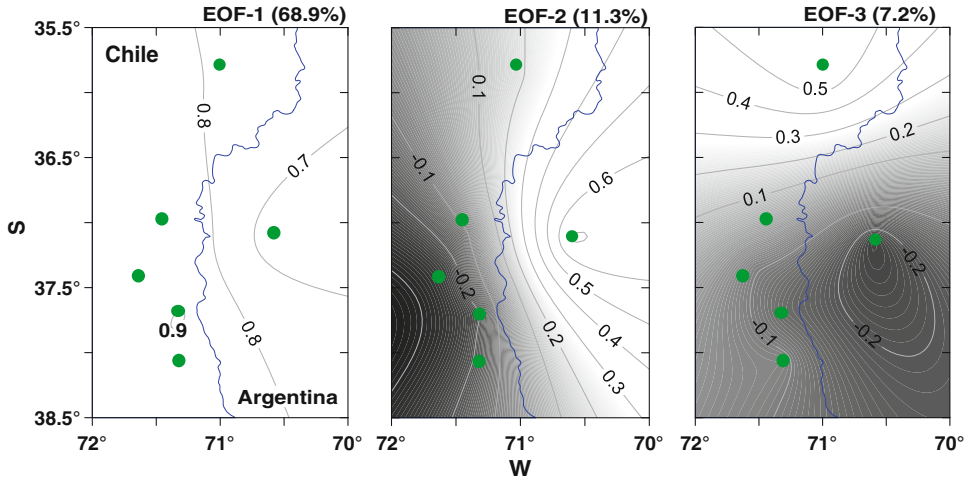

Fig. 3 Empirical Orthogonal Functions (EOFs) for the three leading eigenvectors of the *A. chilensis* prewhitened tree-ring network across the Temperate-Mediterranean transition of the Andes for the 1663–2000 common period. The fractional variance explained (%) by these three spatial structures is indicated at the upper right corner of each map. *Green circles* indicate the location of the tree-ring chronologies. *Isolines* represent the correlation between the principal components of each EOF and the prewhitened tree-ring chronologies. The *blue line* indicates the Chilean-Argentinean border which closely follows the highest elevations of the Andes being the drainage divide of the Cordillera. Correlation coefficients $0.11 < x < -0.11$ are significant at $P < 0.05$ level

evapotranspiration, the amount of water the soil is capable of holding, the amount of moisture that is lost from the soil to evapotranspiration, and runoff (Palmer 1965). We used correlation analysis to define the principal seasonal response of *A. chilensis* to moisture availability by correlating each tree-ring chronology and the first principal component amplitude derived from them with the single grid point from Dai et al. (2004) that had the best geographical match with the narrow latitudinal band of the TMT. The best monthly correlation between our tree-rings and PDSI were during December which corresponds to late-spring early summer (Table 1). Based on these results and because a given month of PDSI integrates current and prior soil moisture conditions over several months (Cook et al. 2007), we choose December as the target instrumental PDSI to be modeled back in time with our tree-rings representing late-spring and early summer moisture conditions. Prior to 1940, the number and quality of temperature and precipitation records in the area preclude the calculation of reliable PDSI indices, resulting in extreme abrupt changes in both the mean and the variance of the PDSI record, which was definitely not a result of climate variability.

Autoregressive modeling (AR) was used to identify the autocorrelation structure of the December PDSI data, which was found to be white noise (AR(0)). To reconstruct this variable with the same autocorrelation structure of the instrumental data, we used tree-ring chronologies which were previously prewhitened using an autoregressive model where the AR(p) order was estimated following the

Table 2 Classification of the Palmer Drought SeverityIndex levels as defined by Palmer (1965)

4.00 or more	Extremely wet
3.00–3.99	Very wet
2.00–2.99	Moderately wet
1.00–1.99	Slightly wet
0.50–0.99	Incipient wet spell
0.49 to −0.49	Near normal
−0.50 to −0.99	Incipient dry spell
−1.00 to 1.99	Mild drought
−2.00 to 2.99	Moderate drought
−3.00 to 3.99	Severe drought
−4.00 or less	Extreme drought

Akaike information criterion (AIC; Akaike 1974). The AR(0) of instrumental PDSI reflects the strong interannual variability of soil moisture content in this abrupt climatic transition zone of the Andes. For these reasons, we expect that our reconstruction highlights the high-frequency variability of the PDSI.

We developed the PDSI reconstruction by regressing tree-rings against December PDSI utilizing a Principal Component Regression (PCR) approach (Briffa et al. 1983; Cook et al. 2007). Potential predictors for the reconstruction were those chronologies that correlated with December PDSI with a probability $\alpha = 0.10$ at either lags t, $t + 1$, and $t + 2$ for the 1960–2000 calibration period (Table 1). This predictor structure allows for a 2 years response to climate in some chronologies (Fritts 1976). All chronologies at lag t and some at $t + 2$ were significantly correlated with PDSI and no chronology was significantly correlated at $t + 1$. The tree-ring series significantly correlated with December PDSI were considered as candidate predictors of drought and entered in a principal component analysis to reduce the number of predictors and enhance the common drought signal. Thus, the intercorrelated set of predictors was converted to orthogonal variables reducing the dimension of the regression problem by eliminating the higher-order eigenvectors that explain a small proportion of the variance (Cooley and Lohnes 1971). We used the objective eigenvalue-1 rule to eliminate those higher-order eigenvectors (Guttman 1954; Kaiser 1960), and only eigenvectors >1.0 were entered into the stepwise multiple regressions. The selection criterion of the final regression model was the maximum adjusted R^2. In order to use the full length of our tree-ring chronologies and maximize the length of the reconstruction, we utilized the PCR in a nested approach whereby the shorter chronologies already used for reconstruction were dropped out and the PCR procedure was repeated utilizing the remaining longer series (Meko 1997; Cook et al. 2004). Each nested PCR had its own calibration (1960–2000) and verification period (1940–1959), with their respective calibration (explained variance or R^2, CRSQ) and verification (squared Pearson correlation, VRSQ; reduction of error, RE; and coefficient of efficiency, CE) statistics, which implies that these may vary in time. The final reconstruction was created by splicing together the relevant segments from each full period calibrated nested model which successfully passed all verification tests (significant VRSQ, and positive RE and CE). This was carried out only after the mean and the variance of each nested reconstruction were adjusted to that of the most replicated nest which exhibited the highest CRSQ or R^2 in order to avoid artificial changes in variance along the reconstruction due to purely statistical, non-climatic reasons (Cook et al. 2004; Wilson et al. 2007). Finally, to reduce the effects of possible underestimate extreme PDSI values by the reconstruction, we restored the lost variance due to regression in the final reconstruction by rescaling it such that its variance over the calibration period was the same as that of the observed PDSI data (Cook et al. 2004).

4 The late-spring early summer PDSI reconstruction: 1346–2002

Figure 4 presents the PDSI reconstruction for the TMT of the Andes spanning the period 1346–2002. The overall Pearson correlations between reconstructed and observed PDSI values were 0.72 and 0.68 for the calibration (1960–2000) and verification periods (1940–1959), respectively (Fig. 4a). The final reconstruction was created from 6 nested subsets of models which successfully passed all verification statistics (significant VRSQ, and positive RE and CE) and the explained climatic variance was in every case highly significant, accounting for 51% (2002–1999), 52% (1998–1663), 49% (1662–1489), 45% (1488–1433), 37% (1432–1429), and 33% (1428–1346) of the instrumental PDSI during the calibration period (R^2_{adj} adjusted for loss of degrees-of-freedom; Draper and Smith 1981). The Durbin-Watson test indicates that the regression residuals were not significantly autocorrelated for any of the models (results not shown). The comparison of the running 41 years variance for the six PDSI reconstructions over their common 1663–1998 period demonstrate a remarkably similarity in the temporal changes of interannual variability among the reconstructed models indicating that in general each one is capturing the same year-to-year changes in moisture variability, which allows the development of a coherent nested reconstruction (Fig. 4b). The comparison of the observed and reconstructed PDSI demonstrate that the tree-ring reconstruction is generally quite accurate in representing the change from wet to dry conditions highlighting the predictive ability of the calibration models

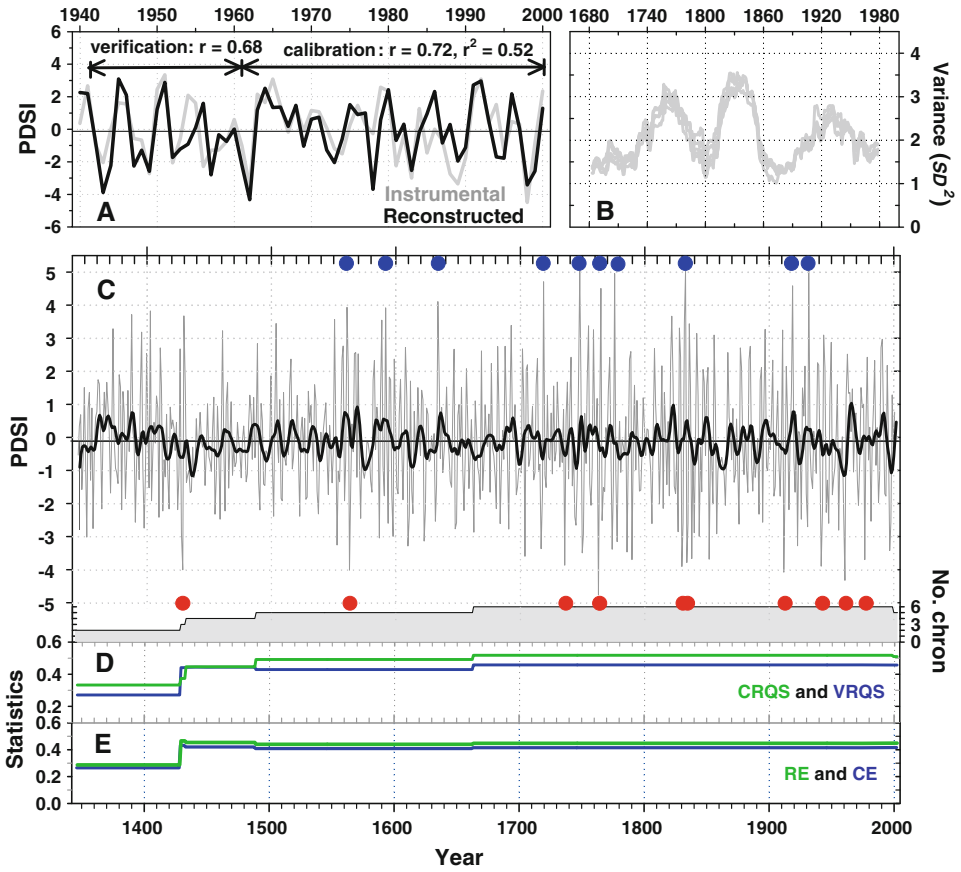

Fig. 4 The tree-ring reconstruction of the late spring–early summer PDSI for the Temperate-Mediterranean transition region of the Andes. **a** Observed and tree-ring predicted December PDSI from 1940 to 2000, **b** comparison of running 41-years variance (SD^2) of the six PDSI reconstruction models for their common 1663–1998 period, **c** reconstructed December PDSI (late-spring early summer) plotted annually from 1346 to 2002 and smoothed with a decadal cubic spline. *Red and blue dots* indicate the ten highest and lowest reconstructed values, respectively. The number of chronologies used for the nested reconstructions through time is also plotted. **d** Calibration and verification statistics for each reconstruction nest: explained variance or R^2 over the calibration period (CRSQ) and the squared Pearson correlation over the verification period (VRSQ), and **e** the reduction of error (RE) and the coefficient of efficiency (CE) over the verification period

(Fig. 4a). Although in general there is a decline in calibration and verification skill of the nested reconstruction as the number of tree-ring predictors available declines, all nested calibration and verification statistics indicate a highly significant hindcast skill of *A. chilensis* to model past late-spring early summer PDSI from the TMT of the Andes.

Examination of the decadal moisture signal of the PDSI reconstruction (Fig. 4c) indicates sustained mild drought conditions during the first half of the fifteenth century, a moderate to severe multi-decadal drought event centered around 1585, moderate drought conditions for the 1640–1670 period, a decadal moderate to severe drought in 1860, and multi-decadal severe drought conditions between 1940 and 1960 with an abrupt change to wetter conditions during the 1960s. This last abrupt decadal scale change is the largest within the reconstruction, with only one possible analog, but with a reversal in conditions from wet to drought, that occurred during the 1565–1585 period.

Superimposed on decadal-scale variability are strong changes in the amplitude of interannual PDSI variability, with an increase in the amplitude after 1740. The period with minor interannual variability within the reconstruction is 1430–1550, which coincides with the longest pluvial spell during the last 700 years of the reconstructed precipitation of the Mediterranean Andes (Le Quesne et al. 2009). Four of the 10 lowest values (1962, 1913, 1943, 1978) and 2 of the 10 highest values (1933, 1920) in the PDSI reconstruction occurred during the twentieth century (Fig. 4c).

Finally, to measure the common variance as a function of frequency between the instrumental and reconstructed PDSI, we conducted a coherence spectral analysis (Jenkins and Watts 1968). This indicates that the PDSI

reconstruction captures the inter-annual and decadal variability in the instrumental data as revealed by the significant squared coherency at 3.5–12 years cycles. These bandwidths contain the largest proportion of the reconstructed variance as is show below (Fig. 5). This indicates that the reconstruction is reproducing the timing and duration of high- to decadal-frequency moisture anomalies.

5 Spatial patterns of PDSI reconstruction in the TMT

To determine the spatial representation of the climatic signal of our PDSI reconstruction and compare it with the one of the instrumental PDSI, we calculated correlation maps comparing the late-spring early summer observed and reconstructed PDSI with the 0.5° × 0.5° gridded late-spring early summer precipitation (November–December) from the CRU TS 2.1 dataset for their 1940–2000 common period (Mitchell and Jones 2005). The comparison between the spatial correlation patterns of precipitation with the instrumental and the reconstructed PDSI demonstrates that our reconstruction captures the regional signal of drought variability in the target region of northwestern Patagonia (Fig. 6). The spatial signal of the reconstructed PDSI mimics the same pattern based on the instrumental PDSI, exhibiting correlations up to 0.7 along the TMT of the Andes. This spatial pattern also resembles the southern portion of the Arid Diagonal on the eastern coast of Patagonia (Abraham et al. 2000).

To characterize the spatial patterns of extreme positive and negative PDSI values within the TMT, we selected the 10 driest (1962, 1943, 1978, 1998, 1924, 1957, 1932, 1949, 1999, 1983) and the 10 wettest years (1933, 1920, 1945, 1992, 1951, 1991, 1964, 1980, 1986, 1940) from the reconstruction within the 1920–2002 period. We choose the 1920–2002 period based on trade-off criterion between

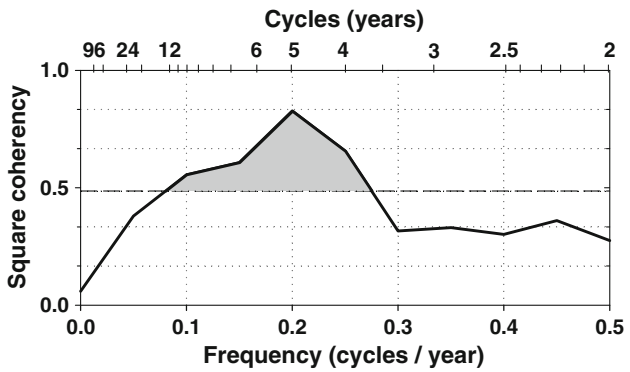

Fig. 5 Coherency spectrum of observed and reconstructed PDSI in the Temperate-Mediterranean transition of the Andes, estimated over the 1940–2002 period. The *short dashed line* indicates the 0.05 probability level

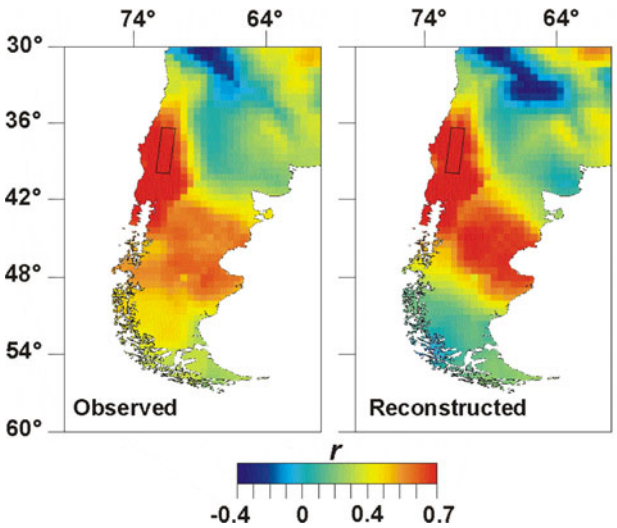

Fig. 6 Spatial correlation fields between the CRU TS 2.1 (Mitchell and Jones 2005) 0.5° × 0.5° gridded November–December precipitation and the observed and reconstructed late-spring early summer (December) PDSI for the 1940–2000 period. Correlation coefficients $0.25 < x < -0.25$ are significant at $P < 0.05$ level. The *black box* indicates the tree-ring sampling area in the Temperate-Mediterranean transition of the Andes

the length and the quality of the 0.5° × 0.5° gridded precipitation series (Mitchell and Jones 2005), and by 1920 an adequate number of precipitation stations in southern South America are available. Based on the 10 (+) and (−) moisture extremes, we created two separate composite maps of the late spring–early summer precipitation by averaging the individual CRU TS 2.1 precipitation grids of the 10 selected years for each moisture extreme. The patterns that emerge from these composite maps clearly indicate the north–south and east–west precipitation gradients of the TMT in both the wettest and driest years (Fig. 7). The main feature displayed by the extreme moisture conditions is the latitudinal shift in the Mediterranean pattern to the south and Temperate rain pattern to the north during the dry and wet events, respectively (Fig. 7). This north–south displacement in the amount of interannual precipitation is what climatically defines the TMT of the Andes, and is a consequence of the latitudinal position of the storm tracks forced by large-scale circulation modes. The reconstruction of PDSI represents this north–south spatial moisture oscillation in the TMT (Fig. 4c), with the negative (positive) PDSI values simulating the Mediterranean (Temperate) pattern (Fig. 7).

6 Temporal evolution of moisture extremes

The PDSI reconstruction of the TMT of the Andes is characterized by high-interannual variability embedded within decadal oscillations. A detailed analysis of the

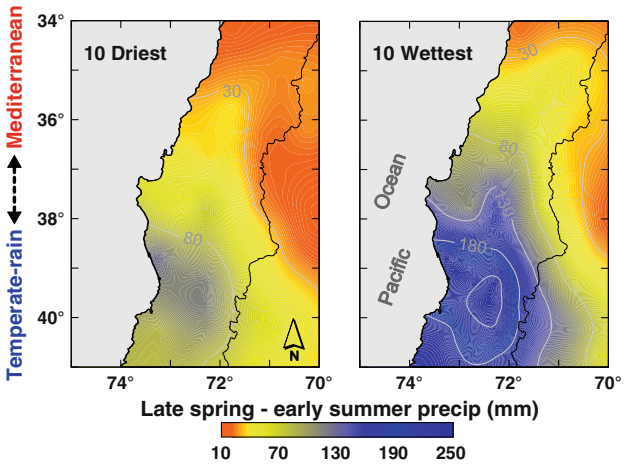

Fig. 7 Composite late-spring early summer (November–December) precipitation (mm) maps from the 0.5° × 0.5° gridded CRU TS 2.1 dataset (Mitchell and Jones 2005) for the 10 driest (in order: 1962, 1943, 1978, 1998, 1924, 1957, 1932, 1949, 1999, 1983) and the 10 wettest years (in order: 1933, 1920, 1945, 1992, 1951, 1991, 1964, 1980, 1986, 1940) in the PDSI reconstruction of the Temperate-Mediterranean transition of the Andes from 1920 to 2002. Contour lines every 50 mm of are indicated. The *black line* represents the Chilean-Argentinean border which closely follows the highest Andean elevations being the continental divide

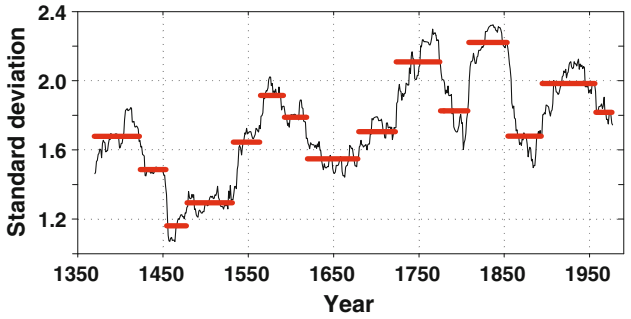

Fig. 8 Changes in standard deviations (SD) across the PDSI reconstruction. SD were calculated for 50-year intervals and plotted on the centroid + 1 year for each interval. The *horizontal red lines* show significant (95% CL) regime shifts in the time series utilizing the Rodionov (2004) method (window length = 50 years)

interannual variability shows remarkable changes in variance in the reconstruction. Periods of extreme high- or more stable-interannual variability alternate across the record, as revealed by changes in the standard deviation (SD) calculated using a 50-years moving window over the 1346–2002 period (Fig. 8). As the different nested models show similar changes in their respective variance through time (Fig. 4b), the changing variance regimes in the reconstruction are likely caused by climate variability. We utilized the Rodionov (2004) method with a window length of 50 years to identify significant shifts in the 50-years moving window of standard deviations across the reconstruction. Figure 8 shows the SD for the full PDSI reconstruction with all significant (95% CL) shifts identified. A clear increase in the interannual moisture variability in the TMT since ~1730 was observed, with three significant and unprecedented ~30 years long peaks centered on 1750, 1849, and 1940. Each peak was followed by a decrease in SD lasting 15–25 years. The decline in variance after 1950 is associated with the increase (decrease) in extreme negative (positive) PDSI values during the same period (Fig. 4c). This reduction in variance, as well as the three characteristic peaks mentioned above, is also present in tree-ring reconstructed precipitation for northern Patagonia (Villalba et al. 1998). Another interesting feature is the decrease in interannual moisture variations during the 1450–1540 period. The lowest period of interannual moisture variability in the reconstruction (1450–1540) is coincident with the longest pluvial period in the Mediterranean Andes during the last 712 years, as reconstructed by a completely independent *A. chilensis* tree-ring network (Le Quesne et al. 2009).

The PDSI reconstruction suggests an increase in the recurrence of droughts during the twentieth century. To assess the occurrence rate of severe and extreme droughts along the reconstruction, we employed a kernel estimation technique (Mudelsee et al. 2003, 2004; Girardin et al. 2006). This method allows the detection of non-linear and non-monotonic trends and does not impose parametric restrictions. We applied a Gaussian kernel estimation to the PDSI extreme dates using a kernel bandwidth of 80 years (obtained via cross-validation and imposing slight undersmoothing) and pseudodata generation rule 'reflection' to reduce boundary bias (Mudelsee et al. 2004). Confidence bands at the 90% level were obtained by 2000 bootstrap resampling steps (Cowling et al. 1996; Mudelsee et al. 2004). The results indicate that the occurrence rate of severe and extreme droughts (PDSI ≤ -3) in the Temperate-Mediterranean transition of the Andes steadily increased between sixteenth and eighteenth centuries, remained constant during the nineteenth century, and significantly increased during the twentieth century ($P < 0.01$; Fig. 9). This increase in drought severity during the last century in the Temperate-Mediterranean transition of the Andes is consistent with Le Quesne et al. (2006), who based on an independent tree-ring network from the Mediterranean region of the Andes, registered a significantly increase in droughts during the twentieth century in the context of the past 800 years.

7 Tropical and high-latitude ocean-atmospheric forcings

To examine the relationship between moisture variability in the TMT and tropical and high-latitude atmospheric

forcings we first performed monthly and seasonal Pearson correlations between the instrumental PDSI, the sea surface temperature (SST) from the Niño-3.4 region (N3.4), and the Antarctic Oscillation Index (AAO) for their common 1950–2001 period. The N3.4 SST is the mean monthly SST anomalies from the N3.4 region of the east-central tropical Pacific at 5°N–5°S, 170°–120°W and was used as an indicator of ENSO behavior (Trenberth 1997). The AAO index is the leading principal component of 850 hPa geopotential height anomalies south of 20°S and is the principal mode of variability of the atmospheric circulation in the southern hemisphere extratropics (Thompson and Wallace 2000; Trenberth et al. 2007). Positive values in the AAO are associated with decreased geopotential height over the Antarctica, increased geopotential height over the mid-latitudes, a poleward shift of the storm track, and a strengthening of the polar vortex. The opposite conditions occur during negative AAO phases (Thompson and Wallace 2000; Fyfe 2003). All correlations were assessed after the red noise was removed from the N3.4 and AAO time series, by prewhitening the time series using an AR model where the order was estimated by means of AIC (Akaike 1974), in order to prevents the adjustment of degrees-of-freedom for the serial persistence seen in the original data to properly test correlation significances (e.g., Dawdy and Matalas 1964).

Correlation results indicate that moisture variability in the TMT of the Andes is significantly and positively related to N3.4 SST during spring with October and November reaching the highest values, which indicates that El Niño (La Niña) conditions are related to wet (dry) conditions in our study region (Fig. 10a). These results are in agreement with previous studies that demonstrated that in our study region the ENSO influence over precipitation occurs during spring, with circulation anomalies during El Niño events

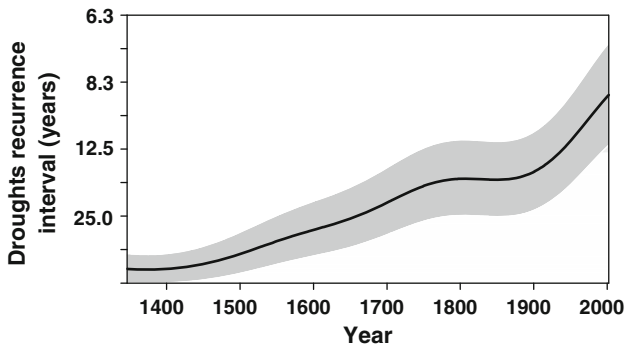

Fig. 9 Occurrence rate (year) of severe and extreme late spring–early summer droughts in the Temperate-Mediterranean transition of the Andes for the 1346–2002 period (*solid black line*) using a Gaussian kernel technique with 90% confidence interval (*shaded*) from 2,000 bootstrap simulations. The extreme event dates are defined by means of a threshold which represent severe and extreme droughts (PDSI ≤ -3). See Table 2 for definition of PDSI levels

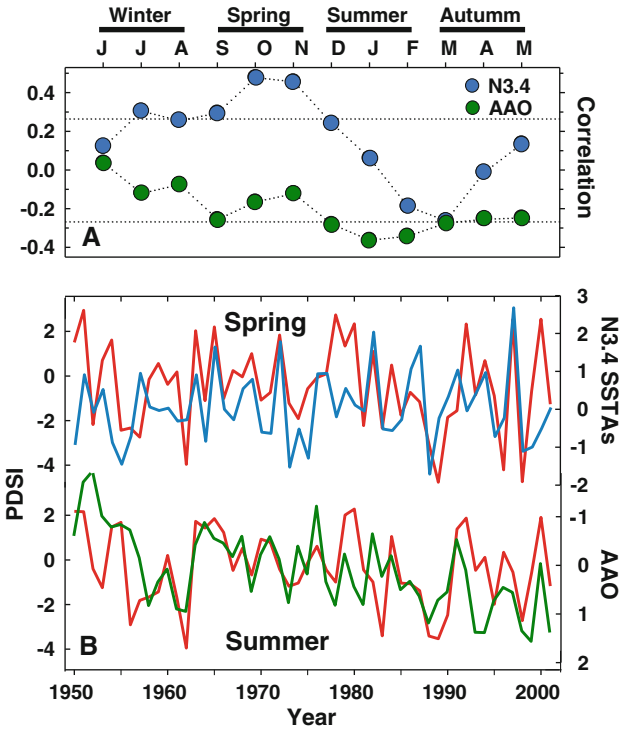

Fig. 10 Comparisons of PDSI and large-scale synoptic indices. **a** Sliding monthly correlations of PDSI with prewhitened SST anomalies of Niño-3.4 region (N3.4) and the prewhitened Antarctic Oscillation index (AAO) for the common 1950–2001 period. *Dashed horizontal lines* indicate statistical significance at the 95% confidence level. **b** Comparisons of mean spring (SON) PDSI and N3.4 SST anomalies and mean summer (DJF) PDSI and AAO for the common 1950–2001 period. Correlations over prewhitened (AR(0)) series are +0.42 for N3.4 and −0.57 for AAO, respectively ($P < 0.01$). Note that the AAO index has been inverted to facilitate the comparison with the PDSI record. Indices colors are similar in (**a**) and (**b**)

characterized by a relatively weak subtropical anticyclone in the southeastern (SE) Pacific, positive SST anomalies in the central tropical Pacific, a warmer than-average troposphere over the tropical Pacific, and strengthened westerly flow in the subtropics off the coast of central Chile, and the reversed pattern during La Niña conditions (Montecinos and Aceituno 2003; Garreaud et al. 2009). Interestingly, the positive relationship between ENSO and PDSI during the spring season vanishes in summer and the AAO becomes significant and negatively correlated with moisture variability in the TMT of the Andes (Fig. 10a). Separate correlations between the N3.4 SST and AAO indicates that they are not intercorrelated during any month or season ($P > 0.05$, $n = 52$). If we compare at the interannual timescale the spring and summer PDSI with spring N3.4 and summer AAO, we find that correlations are significant reaching +0.42 during spring for N3.4 and −0.57 during summer for the AAO ($P < 0.01$, $n = 52$; Fig. 10b). The change in the relationship during spring and summer between PDSI and N3.4 and AAO is remarkable,

highlighting the influence of tropical and high-latitude climatic forcings in modulating moisture conditions in the TMT of the Andes.

To examine the influence of tropospheric circulation anomalies on extreme late-spring early summer moisture variations in the TMT of the Andes we used the 2.5° × 2.5° gridded monthly mean 500-hPa geopotential height dataset (1948 to present) from the National Center for Environmental Prediction-National Center for Atmospheric Research (NCEP-NCAR) reanalysis (Kistler et al. 2001). We selected the 10 highest and lowest PDSI values from our reconstruction within the period 1948–2002 and calculated the mean late-spring early summer (November–December) geopotential height anomalies from 1968 to 1996 reference period for each year to create two separate composite 500-hPa height anomaly maps, averaging the 10 highest and lowest PDSI years from the reconstruction. The 500-hPa height anomaly maps show an association, during late-spring early summer, between large-scale tropospheric circulation in the mid- to high-latitudes of the Southern Hemisphere Pacific Ocean and extreme moisture variability in the TMT of the Andes reconstructed using tree-rings (Fig. 11). The most characteristic features that can be observed in the anomaly maps indicates that drought variability in our study region is closely related to blocking activity in the extra-tropical southern Pacific and the Ross–Amundsen Seas (RoAm). Extreme variations of the 500 mb geopotential height in the dipole between the western ~30°–55°S Pacific and the Ro–Am and surrounding Antarctica appear to influence extreme moisture conditions in the TMT of the Andes. The 10 driest years on record correspond to the regions of averaged negative and positive height anomalies centered between 70° and 80°S, 120° and 150°W (RoAm Seas) and 40° and 50°S, 145° and 160°W in the subtropical Pacific, with in addition, weaker positive height anomalies centered over northern Patagonia (Fig. 11a). Conversely, the 10 wettest years on record correspond to the opposite patterns, with negative 500-hPa geopotential height anomalies in the extra-tropical Pacific centered between 40° and 50°S with two major centers, one in central Patagonia and off the western coast of South America and the most negative off the eastern coast of New Zealand, and an extensive region of averaged positive height anomalies centered between 73° and 80°S, 140°E and 120°W (RoAm; Fig. 11b). These positive (negative) height anomalies over Antarctic circumpolar latitudes produce the northward (southward) migration of the westerly storm track resulting in anomalously wet (dry) conditions over our study region (Pittock 1980; Villalba et al. 1997; Gillett et al. 2006; Garreaud et al. 2009).

The above results indicate that the tree-ring reconstruction is capturing the tropospheric circulation signals

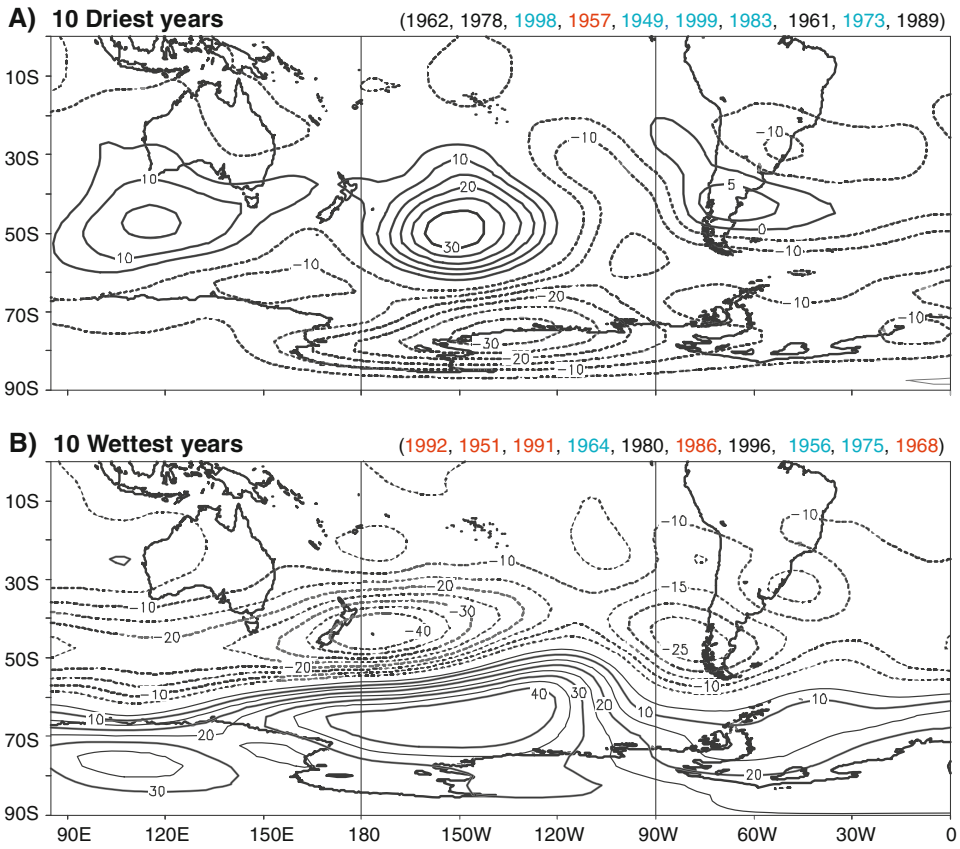

Fig. 11 Composite late-spring early summer (November–December) mean 500-hPa geopotential height anomalies for **a** the 10 driest and **b** the 10 wettest PDSI reconstructed years from the 1948–2002 period. Mean monthly gridded data were obtained from the NCEP–NCAR reanalysis global dataset (Kistler et al. 2001). Contours are in meters with a 5-m contour interval, and zero lines are omitted. Positive (negative) contour anomalies are shown as *solid* (*dashed*) *lines*. *Black, red and light blue* years indicate neutral, El Niño and La Niña events, respectively following Trenberth (1997). Note that drought variability in our study area is closely related to blocking activity in the extra-tropical Pacific and the Ross–Amundsen Seas

that influence late-spring early summer moisture variability in the TMT of the Andes and hence *A. chilensis* growth. The high-latitude geopotential height patterns presented in Fig. 11 are coincident with AAO-like patterns and highlight the positive (negative) effects of high (low) pressure anomalies of high latitudes (i.e. $>\sim 60°S$) on moisture conditions in our study region, corroborating the strong negative correlation between the AAO and PDSI during late-spring early summer in the TMT of the Andes. Only 50% of the 10 wettest (driest) years are coincident with El Niño (La Niña), and also 30% of the 10 wettest years occurred during La Niña events (Fig. 11). The latter, together with the blocking position in the RoAm seas during the wettest years, westward from the typical pattern of El Niño years (Montecinos and Aceituno 2003), suggest along with the correlations from Fig. 10 that the influence of ENSO on late spring–early summer TMT moisture variability is weaker than the AAO.

8 Cycles in reconstructed TMT PDSI

To identify the dominant oscillatory modes in our late-spring early summer PDSI reconstruction and localize changes in the periodicities across the record we performed a continuous Wavelet Transform analysis (WT; Torrence and Compo 1998). The WT reveal non-stationary periodicities across the reconstruction with most spectral power centered within the high-frequency domain (Fig. 12a). Significant increases in interannual moisture variability were recorded during the period 1550–1620 and since ~ 1730. In particular, interannual variability during the last period is clearly unprecedented in the context of the previous reconstructed centuries. Interestingly, the WT of the precipitation reconstruction from the Mediterranean Andes (31°–35°S) which is based in a totally independent tree-ring network, show a similar "silence" of reduced interannual variability prior to 1550, the increase of spectral power between 1550 and 1620 and finally an unprecedented increase in the interannual variability since the end of the 1700s (see Le Quesne et al. 2009).

Because the PDSI reconstruction is recording drought variability in the transition zone between the Mediterranean and Temperate rain climate of the Andes, we compared the spectral properties of the PDSI of our reconstruction with tree-ring based hydroclimatic records from the Mediterranean and Temperate regions of the Andes during their common 1600–2000 period to look for any multicentury relationships. For this purpose we used the past Mediterranean precipitation (31°–35°S) record from Le Quesne et al. (2006) and the Puelo river flow reconstruction from the Temperate Rain Andes which is representative of Northwestern Patagonia riverflows (38°–45°S; Lara et al. 2008). These two reconstructions are

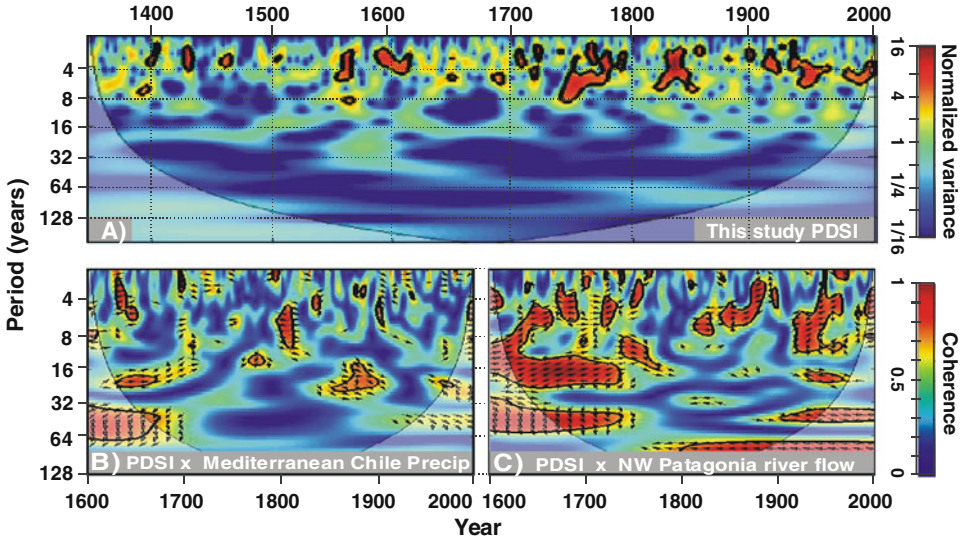

Fig. 12 Spectral properties of the PDSI reconstruction compared with other hydroclimatic tree-ring reconstructions immediately to the north (Mediterranean climate) and south (Temperate climate) of our study region. These reconstructions are based in different tree-ring networks and do not share any tree-ring series between them. **a** The wavelet power spectrum (Morlet) of our PDSI reconstruction, and the wavelet coherency and phase between the TMT PDSI reconstruction and **b** the Mediterranean Chile precipitation reconstruction from Le Quesne et al. (2006) (31°–35°S) and **c** the Northwestern Patagonia river flow reconstruction from Lara et al. (2008) (38°–45°S). The vectors indicate the phase difference between our PDSI reconstruction and the Mediterranean Chile precipitation and NW Patagonia river flow (*an arrow pointing right and left* implies in-phase and anti-phase relationships, respectively, and pointing up means the second series lag the first by 90°). In all panels, *the thick black contours* indicate the 95% significance level using the red noise model, and the cone of influence is shown as a *lighter shade*

based in completely different tree-ring networks, which do not share any tree-ring series between them nor with our PDSI reconstruction. We employed a Wavelet Coherence analysis (WTC; Grinsted et al. 2004) to asses the temporal relationships between our PDSI reconstruction from the TMT and the above palaeohydroclimatic records from the Mediterranean and Temperate Rain Andes. The WTC analysis finds regions in time frequency space where two time series co-vary but not necessarily with high spectral power, and examine if they present a consistent phase relationship to determine whether they are physically related (Grinsted et al. 2004). Monte Carlo methods were used to assess the statistical significance against red noise backgrounds. As we expected, the WTC's results revealed that our PDSI reconstruction show intermittent spectral coherence with both the Mediterranean and Temperate hydroclimate records over the last 400 years, but in general is more closely associated with the Temperate streamflow (Fig. 12c, d). These results indicate that PDSI from the TMT of the Andes may be, at least intermittently, physically related to the two other northern and southern reconstructions that reflect contrasting climate regimes.

At present, the positive and strong ENSO influence on precipitation and snowfall in the Mediterranean Andes is well known (Aceituno 1988; Montecinos and Aceituno 2003; Masiokas et al. 2006; Garreaud et al. 2009), however high-latitude influences have recently been suggested as those responsible for the decreasing trend of the 20th century (Vuille and Milana 2007). Conversely, regional hydroclimate variability in the Temperate Rain Andes is weaker and negatively related to ENSO (Montecinos and Aceituno 2003; Garreaud et al. 2009), and strongly and negatively associated with the AAO which has also been suggested as the main driver of the recent decreasing trend in regional hydroclimate (Lara et al. 2008; Garreaud et al. 2008). The common spectral coherence between the two WTC's may reflect the high-latitude AAO-like forcing operating over the hydroclimate across the South-Central Andes.

9 Discussion and concluding remarks

The Andes Cordillera is one of the largest mountain ranges on earth and acts as a "water tower" for millions of people in South America. In the Central Andes (16°–24°S), abrupt climate changes during the Holocene towards more arid conditions have had critical consequences for past human cultures (Binford et al. 1997; Messerli et al. 2000; Núñez et al. 2002). Today water resources from the TMT of the Andes support a large human population, generate most of the Chilean hydropower, and are the main limiting factor sustaining a fragile and unique ecosystem already highly impacted by anthropogenic activity. Thus, research focused on climate change, with an emphasis on the mechanisms and causes of droughts across this portion of the Andes remain an important research topic. During the last decade considerable scientific progress on climate-forcing and climate variability has been achieved in this region. They include the establishment of close connections between ENSO and regional precipitation (Montecinos and Aceituno 2003), the reconstruction of the past 160 years of precipitation (Lara et al. 2001), the documentation of an increase in elevation of the 0°C isotherm (Carrasco et al. 2008), the detection of regional glacier retreat (Masiokas et al. 2009b), and the decline in regional precipitation records (Carrasco et al. 2005). However, none of the studies have dealt with the variations in aridity conditions at the multi-century time-scale.

This paper represents the first attempt to reconstruct past multi-century aridity changes (PDSI) in the TMT of the Andes. Based on a totally new network of *A. chilensis* chronologies, our reconstruction is also the first estimate of past PDSI fluctuations in the Southern Hemisphere. Our study has provided novel insight into the climate of the TMT of the Andes through (1) a description of late spring–early summer moisture variations for the past 6–7 centuries, (2) the analyses of the spatial patterns of drought variability, (3) an assessment of the links between droughts and tropical to high-latitude ocean-atmospheric forcings, and (4) the comparison of the moisture variations from the TMT with other tree-ring based hydroclimatic records of the last 400 years from the adjacent Mediterranean and Temperate Andes.

Our PDSI reconstruction provides long-term climatic information for a transitional biome in the southern Andes (Fig. 6), where the main characteristic is the strong interannual oscillations in the amount of precipitation (Fig. 7). During dry (wet) years the Mediterranean-like (Temperate rain) pattern extends to the south (north), which can be explained in terms of a reduction (enhance) of the zonal flow at mid-latitudes (Garreaud et al. 2009). The amplitude of these north–south moisture oscillations has fluctuated within higher interannual variability since $\sim$1730 (Figs. 8, 12a). The previous period of lower interannual variability coincides with the well described interval in the northern Temperate Andes of cold-moist conditions from AD 1270 to 1660 reaching its peak around 1340 and 1640 and turning to warmer conditions after 1720 (Villalba 1990), coinciding with the culmination of the major event of the Little Ice Age in Southern Patagonia (Masiokas et al. 2009a). The lowest period of interannual moisture variability in our PDSI reconstruction (1450–1540; Fig. 8) is coincident with the longest pluvial spell in the Mediterranean Andes during the last 700 years, both records sharing extreme low level variability within the high-frequency domain during this

period (Le Quesne et al. 2009). Across the Mediterranean and Temperate Rain Andes, the amplitude of interannual variability of the normalized precipitation is inversely correlated with latitude, with year-to-year variations in the Mediterranean (Temperate) Andes constituting a large (small) fraction of the corresponding annual mean (Garreaud et al. 2009).

Changes in the amplitude and frequency of ENSO are not enough to explain, in the context of the past six centuries, the unprecedented increase in extreme drought events during the twentieth century along the TMT of the Andes (Fig. 9). On the contrary, it has been proposed that the more pronounced El Niño conditions during the last few decades related to wet spells have alleviated dry conditions in the region (Vuille and Milana 2007). The close relationship between negative 500 mb geopotential anomalies in the RoAm Seas and the occurrence of extreme dry events in our reconstruction (Fig. 11), suggests that the AAO is governing moisture conditions in our study region (Yin 2005; Gillett et al. 2006; Chen and Held 2007; Garreaud et al. 2009). Observational data and modeling studies indicate that the anthropogenic ozone depletion and the greenhouse gases increase are the main factors driving the positive trend of the AAO (Thompson and Solomon 2002; Gillett and Thompson 2003; Cai et al. 2003; Marshall et al. 2004; Shindell and Schmidt 2004; Arblaster and Meehl 2006). In response to increasing concentrations of greenhouse gases and tropospheric sulfate aerosols, the most recent multi-model analyses (Miller et al. 2006), simulate the continuation of the persistent positive trend in the AAO during late-spring and summer (November–February), the period with the strongest influences of the AAO on TMT-PDSI (Figs. 10b, 11). This pattern of change towards decreasing Antarctic SLP is linked to a poleward shift of the mid-latitude storm tracks (Yin 2005) and the intensification of aridity in the TMT of the Andes (Christensen et al. 2007; Fuenzalida et al. 2007). The observed steadily increment in the occurrence of extreme droughts in our PDSI reconstruction since the pre-industrial era indicates that anthropogenic changes in the AAO may be interacting with the natural variability and causing more arid conditions in the TMT of the Andes.

According to the very likely future increase in Mediterranean-like conditions in the TMT, the current knowledge of *Austrocedrus* climate–growth relationships and the effect of drought events on recruitment and mortality rates, the population dynamics of this species at its ecological boundary could be severely affected by a future increase in extreme drought events (Villalba and Veblen 1997, 1998; Tercero-Bucardo et al. 2007). The implementation of future monitoring programs of rare and endemic species in the TMT hotspot as a response to climate variability should be implemented. The predicted increase in drought conditions in the TMT of the Andes will also have negative socioeconomic implications, especially on the highly water-dependent Chilean economy. These threatened changes highlight the need for future research into the possible interactions between AAO and ENSO on drought variability in this region. It is a challenge to develop and implement validation techniques of the current climate models for this region based on annually resolved tree-ring drought reconstructions. This first PDSI reconstruction for South America demonstrates the highly significant hindcast skill of *A. chilensis* as an aridity proxy. Future research will be focused on exploring low-frequency drought signals and enhancing the current tree-ring network to develop a gridded PDSI reconstruction across the Mediterranean and Temperate Rain regions of south-western South America. This expanded network of proxy tree-ring reconstructions will capture a wider range of tropical and high-latitude climate forcings on moisture conditions over a broad portion of the southern Andes.

Acknowledgments This work was carried out with the aid of grants from the Inter-American Institute for Global Change Research (IAI) CRN II # 2047 supported by the US National Science Foundation (GEO-0452325), Universidad Austral de Chile (DID-UACh D-2007-07), Chilean Research Council (FONDECYT 1050298 and FONDECYT PDA-24), Chilean Ministry of Planning (ICM project P04-065-F), and the Argentinean Agency for Promotion of Science (PICTR 02-186). We are grateful to D. Shea from the NCAR Climate and Global Dynamics Division for providing the Niño-3.4 region SST record extracted from Hurrell et al. (2008). The AAO data were obtained from Joint Institute for the Study of the Atmosphere and Ocean (JISAO; http://jisao.washington.edu/data/aao/). Other than the first author, order of authorship is alphabetical. D. C. is grateful to M[a] Paz Peña, Natalia Carrasco and Mauricio Fuentes for their great help during fieldwork and Jonathan Barichivich for helpful discussion about this research. We acknowledge Chilean Forest Service CONAF, Juan Manquepi, Lito Cáceres, and Comunidad Pehuenche Ralko-Lepoy for permission to collect *A. chilensis* samples.

References

Abraham EM, Garleff K, Liebricht H, Regairaz AC, Schaebitz F, Squeo FA, Stingl H, Villagrán C (2000) Geomorphology and paleoecology of the arid diagonal in southern South America. Z Angew Geol SH1:55–61

Aceituno P (1988) On the functioning of the Southern Oscillation in the South American sector. Part I: surface climate. Mon Weather Rev 116:505–524. doi:10.1175/1520-0493(1988)116<0505:OTFOTS>2.0.CO;2

Aceituno P, Fuenzalida H, Rosenbluth B (1983) Climate along the west coast of South America. In: Mooney HA, Fuentes ER, Kronber BI (eds) Earth system responses to global change: contrasts between North and South America. Academic Press Inc, California, pp 61–69

Akaike H (1974) A new look at the statistical model identification. IEEE Trans Automat Contr AC-19:716–723. doi:10.1109/TAC.1974.1100705

Arblaster JM, Meehl GA (2006) Contributions of external forcings to Southern Annular Mode trends. J Clim 19:2896–2905. doi:10.1175/JCLI3774.1

Armesto JJ, Villagrán C, Kalin M (1996) Ecología de los bosques nativos de Chile. Editorial Universitaria, Santiago

Binford MW, Kolata AL, Brenner M, Janusek JW, Seddon MT, Abbott MB, Jason H (1997) Climate variation and the rise and fall of an Andean civilization. Quat Res 47:235–248. doi:10.1006/qres.1997.1882

Boninsegna JA (1988) Santiago de Chile winter rainfall since 1220 as being reconstructed by tree rings. Quat S Am Antarct Penins 7:315–326

Boninsegna JA, Holmes R (1978) Breve descripción de un relicto de *Austrocedrus chilensis* (D. Don) Endl. en Huinganco (Pcia. del Neuquén). Anales Instituto Argentino de Nivología y Glaciología 4:115–123

Boninsegna JA, Argollo J, Aravena JC, Barichivich J, Christie D, Ferrero ME, Lara A, Le Quesne C, Luckman BH, Masiokas M, Morales M, Oliveira JM, Roig F, Srur A, Villalba R (2009) Dendroclimatological reconstructions in South America: a review. Palaeogeogr Palaeoclimatol Palaeoecol 281:210–228. doi:10.1016/j.palaeo.2009.07.020

Bradley RS, Vuille M, Diaz HF, Vergara W (2006) Threats to water supplies in the tropical Andes. Science 312:1755–1756. doi:10.1126/science.1128087

Briffa KR, Jones PD, Wigley TML, Pilcher JR, Baillie MGL (1983) Climate reconstruction from tree rings: part 1, basic methodology and preliminary results for England. Int J Climatol 3:233–242. doi:10.1002/joc.3370030303

Bustamante R, Castor C (1998) The decline of an endangered ecosystem: the Ruil (*Nothofagus alessandrii*) forest in Central Chile. Biodivers Conserv 7:1607–1626

Cai W, Whetton PH, Karoly DJ (2003) The response of the Antarctic Oscillation to increasing and stabilized atmospheric CO_2. J Clim 16:1525–1538. doi:10.1175/1520-0442(2003)016<1525:TROTAO>2.0.CO;2

Camus P (2006) Ambientes, bosques y gestión forestal en Chile: 1541–2005. Centro de Investiagciones Diego Barros Arana, LOM ediciones, Santiago

Carrasco JF, Casassa G, Quintana J (2005) Changes of the 0°C isotherm and the equilibrium line altitude in central Chile during the last quarter of the 20th century. Hydrol Sci J 50:933–948

Carrasco JF, Osorio R, Casassa G (2008) Secular trend of the equilibrium-line altitude on the western side of the southern Andes, derived from radiosonde and surface observations. J Glaciol 54:538–550. doi:10.3189/002214308785837002

Chen G, Held IM (2007) Phase speed spectra and the recent poleward shift of Southern Hemisphere surface westerlies. Geophy Res Lett 34:L21805. doi:10.1029/2007GL031200

Christensen JH, Hewitson B, Busuioc A, Chen A, Gao X, Held I, Jones R, Kolli RK, Kwon WT, Laprise R, Magaña Rueda V, Mearns L, Menéndez CG, Räisänen J, Rinke A, Sarr A, Whetton P (2007) Regional climate projections. In: Solomon S, Qin D, Manning M, Chen Z, Marquis M, Averyt KB, Tignor M, Miller HL (eds) Climate change 2007: the physical science basis. Contribution of Working Group I to the Fourth Assessment Report of the Intergovernmental Panel on climate change. Cambridge University Press, Cambridge, pp 847–940

Cobos DR, Boninsegna JA (1983) Fluctuations of some glaciers in the Upper Atuel river basin, Mendoza, Argentina. Quat S Am Antarct Penins 1:61–82

Cook ER, Krusic PJ (2006) Program ARSTAN: a tree-ring standardization program based on detrending and autoregressive time series modeling, with interactive graphics. Tree-Ring Laboratory Lamont Doherty Earth Observatory of Columbia University Palisades, NY

Cook ER, Woodhouse CA, Eakin CM, Meko DM, Stahle DW (2004) Long-term aridity changes in the western United States. Science 306:1015–1018. doi:10.1126/science.1102586

Cook ER, Saeger R, Cane M, Stahle DW (2007) North American drought: reconstructions, causes, and consequences. Earth Sci Rev 81:93–134

Cooley WW, Lohnes PR (1971) Multivariate data analysis. Wiley, New York

Cortés G, Vargas X, McPhee J (2008) Evidence of climate change in streamflow timing in the western slope of the Southern Andes Cordillera during the 1961–2006 period. EGU Topical Conference Series 4th Alexander von Humboldt International Conference: the Andes Challenge for Geosciences. Santiago

Cowling A, Hall P, Phillips MJ (1996) Bootstrap confidence regions for the intensity of a Poisson point process. J Am Stat Assoc 91:1516–1524

Dai A, Trenberth KE, Qian T (2004) A global dataset of Palmer drought severity index for 1870–2002: relationship with soil moisture and effects of surface warming. J Hydrometeorol 5:1117–1130. doi:10.1175/JHM-386.1

Dawdy DR, Matalas NC (1964) Statistical and probability analysis of hydrologic data. Part III. Analysis of variance, covariance, and time series. In: Chow VT (ed) Handbook of applied hydrology: a compendium of water-resources technology. McGraw-Hill, New York, pp 8.68–8.90

Dillehay TD (2007) Monuments, resistance and Empires in the Andes: Araucanian ritual narratives and polity. Cambridge University Press, Cambridge

Draper NR, Smith H (1981) Applied regression analysis. Wiley, New York

Echeverría C, Coomes D, Salas J, Rey Benayas JM, Lara A, Newton A (2006) Rapid deforestation and fragmentation of Chilean temperate forests. Biol Conserv 130:481–494. doi:10.1016/j.biocon.2006.01.017

Fritts HC (1976) Tree rings and climate. Academic Press, London

Fuenzalida H, Aceituno P, Falvey M, Garreaud R, Rojas M, Sanchez R (2007) Study on climate variability for Chile during the 21st century. Technical Report prepared for the National Environmental Committee (CONAMA), Department of Geophysics, Universidad de Chile, 142 pp. Accessed 1 Sept 2009. Available at: http://www.dgf.uchile.cl/PRECIS

Fyfe JC (2003) Separating extratropical zonal wind variability and mean change. J Clim 16:863–874. doi:10.1175/1520-0442(2003)016<0863:SEZWVA>2.0.CO;2

Garreaud R (2007) Precipitation and circulation covariability in the extratropics. J Clim 20:4789–4797. doi:10.1175/JCLI4257.1

Garreaud RD, Vuille M, Compagnucci R, Marengo J (2009) Present-day South American climate. Palaeogeogr Palaeoclimatol Palaeoecol 281:180–195. doi:10.1016/j.palaeo.2007.10.032

Ghil M, Allen MR, Dettinger MD, Ide K, Kondrashov D, Mann ME, Robertson AW, Saunders A, Tian Y, Varadi F, Yiou P (2002) Advanced spectral methods for climatic time series. Rev Geophys 40:1–41. doi:10.1029/2000RG000092

Giglo N (2006) Informe País: Estado del Medio Ambiente en Chile 2005. Instituto de Asuntos Públicos, Universidad de Chile, LOM ediciones, Santiago

Gillett NP, Thompson DWJ (2003) Simulation of recent Southern Hemisphere climate change. Science 302:273–275. doi:10.1126/science.1087440

Gillett NP, Kell TD, Jones PD (2006) Regional climate impacts of the Southern Annular Mode. Geophys Res Lett 33:L23704. doi:10.1029/2006GL027721

Girardin MP, Bergeron Y, Tardif JC, Flannigan MD, Gauthier S, Mudelsee M (2006) A 229-year dendroclimatic-inferred record of forest fire activity for the Boreal Shield of Canada. Int J Wildland Fire 15:375–388

Grinsted A, Moore JC, Jevrejeva S (2004) Application of the cross wavelet transform and wavelet coherence to geophysical time series. Nonlinear Process Geophys 11:561–566

Guttman L (1954) Some necessary conditions for common-factor analysis. Psychometrika 19:149–161. doi:10.1007/BF02289162

Hegerl GC, Zwiers FW, Braconnot P, Gillett NP, Luo Y, Marengo Orsini JA, Nicholls N, Penner JE, Stott PA (2007) Understanding and attributing climate change. In: Solomon S, Qin D, Manning M, Chen Z, Marquis M, Averyt KB, Tignor M, Miller HL (eds) Climate change 2007: the physical science basis. Contribution of Working Group I to the Fourth Assessment Report of the Intergovernmental Panel on climate change. Cambridge University Press, Cambridge, pp 663–745

Holmes RL (1983) Computer-assisted quality control in tree-ring dating and measurements. Tree Ring Bull 43:69–75

Holmes RL, Stockton CW, LaMarche VC (1979) Extension of river flow records in Argentina from long tree-ring chronologies. Water Resour Bull 15:1081–1085. doi:10.1111/j.1752-1688.1979.tb01086.x

Hurrell JW, Hack JJ, Shea D, Caron JM, Rosinski J (2008) A new sea surface temperature and sea ice boundary data set for the community atmosphere model. J Clim 21:5145–5153. doi:10.1175/2008JCLI2292.1

INE (2004) Anuario estadístico sector eléctrico. Instituto Nacional de Estadísticas de Chile (INE), Santiago

Jansen E, Overpeck J, Briffa KR, Duplessy JC, Joos F, Masson-Delmotte V, Olago D, Otto-Bliesner B, Peltier WR, Rahmstorf S, Ramesh R, Raynaud D, Rind D, Solomina O, Villalba R, Zhang D (2007) Palaeoclimate. Climate Change 2007: The Physical Science Basis. In: Solomon S, Qin D, Manning M, Chen Z, Marquis M, Averyt KB, Tignor M, Miller HL (eds) Climate change 2007: the physical science basis. Contribution of Working Group I to the Fourth Assessment Report of the Intergovernmental Panel on Climate Change. Cambridge University Press, pp 433–497

Jenkins GM, Watts DG (1968) Spectral analysis and its applications. Holden-Day, San Francisco

Kaiser HF (1960) The application of electronic computers to factor analysis. Educ Psychol Meas 20:141–151

Kistler R, Kalnay E, Collins W, Saha S, White G, Woollen J, Chelliah M, Ebisuzaki W, Kanamitsu M, Kousky V, Van den Dool H, Jenne R, Fiorino M (2001) The NCEP-NCAR 50-year reanalysis: monthly means CD-ROM and documentation. Bull Am Meteorol Soc 82:247–267

LaMarche VC (1978) Tree-ring evidence of past climatic variability. Nature 276:334–338. doi:10.1038/276334a0

Lara A, Veblen TT (1993) Forest plantations in Chile: a successful model? In: Mather A (ed) Afforestation policies, planning and progress. Belhaven Press, London, pp 118–139

Lara A, Aravena JC, Villalba R, Wolodarsky-Franke A, Luckman BH, Wilson R (2001) Dendroclimatology of high-elevation *Nothofagus pumilio* forest at higher northern distribution limit in the central Andes of Chile. Can J Forest Res 31:925–936

Lara A, Villalba R, Urrutia R (2008) A 400-year tree-ring record of the Puelo River summer-fall streamflow in the Valdivian Rainforest eco-region, Chile. Clim Change 86:331–356. doi:10.1007/s10584-007-9287-7

Le Quesne C, Stahle DW, Cleaveland MK, Therrell MD, Aravena JC, Barichivich J (2006) Ancient *Austrocedrus* tree-ring chronologies used to reconstruct Central Chile precipitation variability from A.D. 1200 to 2000. J Clim 19:5731–5744. doi:10.1175/JCLI3935.1

Le Quesne C, Acuña C, Boninsegna JA, Rivera A, Barichivich J (2009) Long-term glacier variations in the Central Andes of Argentina and Chile, inferred from historical records and tree-ring reconstructed precipitation. Palaeogeogr Palaeoclimatol Palaeoecol 281:334–344. doi:10.1016/j.palaeo.2009.07.020

Lohmann G (2008) Linking data and models. Past Global Changes PAGES 16:4–5

Marshall GJ, Stott PA, Turner J, Connolley WM, King JC, Lachlan-Cope TA (2004) Causes of exceptional atmospheric circulation changes in the Southern Hemisphere. Geophys Res Lett 31:L14205. doi:10.1029/2004GL019952

Masiokas MH, Villalba R, Luckman BH, LeQuesne C, Aravena JC (2006) Snowpack Variations in the Central Andes of Argentina and Chile, 1951–2005: large-scale atmospheric influences and implications for water resources in the region. J Clim 19:6334–6352. doi:10.1175/JCLI3969.1

Masiokas MH, Luckman BH, Villalba R, Delgado S, Skvarca P, Ripalta A (2009a) Little Ice Age fluctuations of small glaciers in the Monte Fitz Roy and Lago del Desierto areas, south Patagonian Andes, Argentina. Palaeogeogr Palaeoclimatol Palaeoecol 281:351–362. doi:10.1016/j.palaeo.2007.10.031

Masiokas MH, Rivera A, Espizua LE, Villalba R, Delgado S, Aravena JC (2009b) Glacier fluctuations in extratropical South America during the past 1,000 years. Palaeogeogr Palaeoclimatol Palaeoecol 281:242–268. doi:10.1016/j.palaeo.2009.08.006

Meko DM (1997) Dendroclimatic reconstruction with time varying subsets of tree indices. J Clim 10:687–696. doi:10.1175/1520-0442(1997)010<0687:DRWTVP>2.0.CO;2

Messerli B, Grosjean M, Hofer T, Núñez L, Pfister C (2000) From nature-dominated to human-dominated environmental changes. Quat Sci Rev 19:459–479. doi:10.1016/S0277-3791(99)00075-X

Miller A (1976) The climate of Chile. In: Schwerdtfeger W (ed) World survey of climatology. Climates of Central and South America. Elsevier, Amsterdam, pp 113–131

Miller RL, Schmidt GA, Shindell DT (2006) Forced annular variations in the 20th century IPCC AR4 simulations. J Geophys Res 111:D18101. doi:10.1029/2005JD006323

Mitchell TD, Jones PD (2005) An improved method of constructing a database of monthly climatological observations and associated high-resolution grids. Int J Climatol 25:693–712. doi:10.1002/joc.1181

Montecinos A, Aceituno P (2003) Seasonality of the ENSO-related rainfall variability in Central Chile and associated circulation anomalies. J Clim 16:281–296. doi:10.1175/1520-0442(2003)016<0281:SOTERR>2.0.CO;2

Mudelsee M, Börngen M, Tetzlaff G, Grünewald U (2003) No upward trends in the occurrence of extreme floods in central Europe. Nature 425:166–169. doi:10.1038/nature01928

Mudelsee M, Börngen M, Tetzlaff G, Grünewald U (2004) Extreme floods in central Europe over the past 500 years: Role of cyclone pathway ''Zugstrasse Vb''. J Geophys Res 109:D23101. doi:10.1029/2004JD005034

Myers N, Mittermeier RA, Mittermeier CG, da Fonseca GA, Kent J (2000) Biodiversity hotspots for conservation priorities. Nature 403:853–858. doi:10.1038/35002501

Núñez L, Grosjean M, Cartagena I (2002) Human occupations and climate change in the Puna de Atacama, Chile. Science 298:821–824. doi:10.1126/science.1076449

Osborn TJ, Briffa KB, Jones PD (1997) Adjusting variance for sample size in tree-ring chronologies and other regional mean timeseries. Dendrochronologia 15:89–99

Palmer WC (1965) Meteorological drought. Research Paper, vol 45. U.S. Weather Bureau

Pittock AB (1980) Patterns of climatic variation in Argentina and Chile. I. Precipitation, 1931–1960. Mon Weather Rev 108:1347–1361

Randall DA, Wood RA, Bony S, Colman R, Fichefet T, Fyfe J, Kattsov V, Pitman A, Shukla J, Srinivasan J, Stouffer RJ, Sumi A, Taylor KE (2007) Climate Models and Their Evaluation. In: Solomon S, Qin D, Manning M, Chen Z, Marquis M, Averyt KB, Tignor M, Miller HL (eds) Climate change 2007: the physical science basis. Contribution of Working Group I to the Fourth Assessment Report of the Intergovernmental Panel on climate change. Cambridge University Press, Cambridge, pp 489–662

Rodionov SN (2004) A sequential algorithm for testing climate regime shifts. Geophys Res Lett 31. doi:10.1029/2004GL019448

Rodriguez-Cabal MA, Nuñez MA, Martínez AS (2008) Quantity versus quality: endemism and protected areas in the temperate forest of South America. Austral Ecol 33:730–736. doi:10.1111/j.1442-9993.2008.01841.x

Samaniego H, Marquet PA (2009) Mammal and butterfly species richness in Chile: taxonomic covariation and history. Rev Chil Hist Nat 82:135–151. doi:10.4067/S0716-078X2009000100009

Schulman E (1956) Dendroclimatic changes in semiarid America. University of Arizona Press, Tucson

Shindell DT, Schmidt GA (2004) Southern Hemisphere climate response to ozone changes and greenhouse gas increases. Geophys Res Lett 31:L18209. doi:10.1029/2004GL020724

Stokes MA, Smiley TL (1968) An introduction to tree-ring dating. University of Chicago Press, Chicago

Tercero-Bucardo N, Kitzberger T, Veblen TT, Estela R (2007) A field experiment on climatic and herbivore impacts on post-fire tree regeneration in north-western Patagonia. J Ecol 95:771–779. doi:10.1111/j.1365-2745.2007.01249.x

Thompson DWJ, Solomon S (2002) Interpretation of recent Southern Hemisphere climate change. Science 296:895–899. doi:10.1126/science.1069270

Thompson DWJ, Wallace JM (2000) Annular modes in the extratropical circulation. Part I: month-to-month variability. J Climate 13:1000–1016. doi:10.1175/1520-0442(2000)013<1000:AMITEC>2.0.CO;2

Torrence C, Compo GP (1998) A practical guide to wavelet analysis. Bull Am Meteorol Soc 78:61–79. doi:10.1175/1520-0477(1998)079<0061:APGTWA>2.0.CO;2

Trenberth KE (1997) The definition of El Niño. Bull Am Meteorol Soc 78:2771–2777. doi:10.1175/1520-0477(1997)078<2771:TDOENO>2.0.CO;2

Trenberth KE, Jones PD, Ambenje P, Bojariu R, Easterling D, Klein Tank A, Parker D, Rahimzadeh F, Renwick JA, Rusticucci M, Soden B, Zhai P (2007) Observations: Surface and atmospheric climate change. In: Solomon S, Qin D, Manning M, Chen Z, Marquis M, Averyt KB, Tignor M, Miller HL (eds) Climate change 2007: the physical science basis. Contribution of Working Group I to the Fourth Assessment Report of the Intergovernmental Panel on climate change. Cambridge University Press, pp 235–336

Underwood EC, Klausmeyer KR, Cox RL, Busby SM, Morrison SA, Shaw MR (2008) Expanding the global network of protected areas to save the imperiled Mediterranean biome. Conserv Biol 23:43–52. doi:10.1111/j.1523-1739.2008.01072.x

Veblen TT, Young KR, Orme AR (2007) The physical geography of South America. Oxford University Press, Inc., New York

Villagrán C, Hinojosa LF (1997) Historia de los bosques del sur de Sudamérica, II: análisis fitogeográfico. Rev Chil Hist Nat 70:241–267

Villalba R (1990) Climatic fluctuations in northern Patagonia during the last 1,000 years as inferred from tree-ring records. Quat Res 34:346–360. doi:10.1016/0033-5894(90)90046-N

Villalba R, Veblen TT (1997) Regional patterns of tree population age structure in northern Patagonia: climatic and disturbance influences. J Ecol 85:113–124

Villalba R, Veblen TT (1998) Influences of large-scale climatic variability on episodic tree mortality in Northern Patagonia. Ecology 79:2624–2640. doi:10.1890/0012-9658(1998)079[2624:IOLSCV]2.0.CO;2

Villalba R, Cook ER, D'Arrigo RD, Jacoby GC, Jones PD, Salinger MJ, Palmer J (1997) Sea-level pressure variability around Antarctica since A.D. 1750. Clim Dyn 13:375–390. doi:10.1007/s003820050172

Villalba R, Cook ER, Jacoby GC, D'Arrigo RD, Veblen TT, Jones PD (1998) Tree-ring based reconstructions of northern Patagonia precipitation since AD 1600. Holocene 8:659–674. doi:10.1191/095968398669095576

Vuille M, Milana JP (2007) High-latitude forcing of regional aridification along the subtropical west coast of South America. Geophys Res Lett 34:L23703. doi:10.1029/2007GL031899

Wigley TML, Briffa KR, Jones PD (1984) On the average value of correlated time series, with applications in dendroclimatology and hydrometeorology. J Clim Appl Meteorol 23:201–213

Wilson R, Wiles G, D'Arrigo R, Zweck C (2007) Cycles and shifts: 1,300 years of multi-decadal temperature variability in the Gulf of Alaska. Clim Dyn 28:425–440. doi:10.1007/s00382-006-0194-9

Yin JH (2005) A consistent poleward shift of the storm tracks in simulations of 21st century climate. Geophys Res Lett 32:L18701. doi:10.1029/2005GL023684

Young KR, León B (2006) Tree-line changes along the Andes: implications of spatial patterns and dynamics. Phil Trans R Soc B. doi:10.1098/rstb.2006.1986